Materials Science and Engineering B 178 (2013) 1515–1522

Contents lists available at ScienceDirect

Materials Science and Engineering B

journal homepage: www.elsevier.com/locate/mseb

# Physical and electrochemical properties of cobalt doped (Ti,Ru)$O_2$ electrode coatings

Christine Hummelgård[a], Rasmus K.B. Karlsson[b], Joakim Bäckström[a], Seikh M.H. Rahman[c], Ann Cornell[b], Sten Eriksson[c], Håkan Olin[a,*]

[a] Department of Natural Sciences, Mid Sweden University, SE-851 70 Sundsvall, Sweden
[b] Applied Electrochemistry, School of Chemical Science and Engineering, KTH Royal Institute of Technology, SE-100 44 Stockholm, Sweden
[c] Department of Chemical and Biological Engineering, Chalmers University of Technology, SE-412 96 Gothenburg, Sweden

ARTICLE INFO

*Article history:*
Received 25 March 2013
Received in revised form 17 August 2013
Accepted 29 August 2013
Available online 11 September 2013

*Keywords:*
DSA®
Cobaltdoping
XRD
Polarization curves
Hydrogen evolution
Chlorine evolution

ABSTRACT

The physical and electrochemical properties of ternary oxides $Ti_{0.7}Ru_{0.3-x}Co_xO_2$ ($x = 0.093$ and $x = 0$) have been investigated and compared. Samples of three different thicknesses were prepared by spin-coating onto polished titanium to achieve uniform and well-defined coatings. The resulting electrodes were characterized with a variety of methods, including both physical and electrochemical methods. Doping with cobalt led to a larger number of micrometer-sized cracks in the coating, and coating grains half the size compared to the undoped samples (10 instead of 20 nm across). This is in agreement with a voltammetric charge twice as high, as estimated from cyclic voltammetry. There is no evidence of a $Co_3O_4$ spinel phase, suggesting that the cobalt is mainly incorporated in the overall rutile structure of the (Ti,Ru)$O_2$. The doped electrodes exhibited a higher activity for cathodic hydrogen evolution compared to the undoped electrodes, despite the fact that one third of the active ruthenium was substituted with cobalt. For anodic chlorine evolution, the activity was similar for both electrode types.



## 1. Introduction

Transition metal oxides are used for many electrochemical applications, such as gas sensors and chlorine or oxygen evolving electrodes [1]. One of the most commonly used transition metal oxide in catalytic electrode materials is ruthenium dioxide ($RuO_2$). Ruthenium is a relatively expensive metal and is therefore often used as mixed with a variety of other metal oxides. The most common mixture is with titanium dioxide ($TiO_2$) [2], where a purpose of the titanium dioxide also is to enhance the coating stability [3]. Coatings of the standard DSA® composition (30 mol% $RuO_2$ and 70 mol% $TiO_2$) combine a high stability with a high activity and a high selectivity toward chlorine evolution [4,5], and have therefore been used as the primary catalyst in chlorine and chlorate production for over 40 years. Ruthenium dioxide has also been doped with for example Ce [6], Sn [7], Co [8–12] or Ni [13] to improve the catalytic activity, enhance the selectivity and/or increase the stability of the coating. Additions of a third oxide to the ruthenium–titanium mix have been performed to improve the coating properties even further [3,14–17].

The interest for using $Co_3O_4$ as an electrode coating component started in the late 1970s. Agapova and Kokhanov [18] studied the preparation and activity of $Co_3O_4$ electrode coatings, and found a high selectivity for chlorine evolution, as well as Tafel slopes and overpotentials for chlorine evolution similar to those exhibited by DSA® electrodes. A series of studies further examined the composition, morphology and chemical behavior of $Co_3O_4$ coatings during the first half of the 1980s [19–21]. It was concluded that the high activity of $Co_3O_4$ coatings was primarily governed by their large active surface area [21]. Boggio et al. [22] studied the anodic evolution of $Cl_2$ on $Co_3O_4$ and expressed the belief that the difference in activity between $Co_3O_4$ and $RuO_2$ is small enough to make the replacement economically favorable, even though $RuO_2$ is intrinsically more active than the less expensive cobalt oxide. Boggio et al. [23] then further investigated the electrochemical surface properties of $Co_3O_4$ coated electrodes. Although these early studies found that the activity of $Co_3O_4$ was close to that of $RuO_2$, the instability of $Co_3O_4$ in acidic solutions [1] was a serious drawback. Further studies were performed in the 1990s, looking at mixed oxides of $Co_3O_4$ and $RuO_2$ coated on Ni electrodes for hydrogen [24,25] and chlorine evolution [26]. At the beginning of the 2000s more studies appeared on surface characteristics, stability and activities for oxygen and chlorine evolution of mixed coatings of $RuO_2$ and

* Corresponding author. Tel.: +46 60 148855.
*E-mail address:* hakan.olin@miun.se (H. Olin).

0921-5107 
http://dx.doi.org/10.1016/j.mseb.2013.08.018

$Co_3O_4$ [9–11,27]. More recently, nanocrystalline coatings of $RuO_2$ and $Ru_{0.8}Co_{0.2}O_{2-x}$ were investigated using a variety of surface characterization techniques and differential electrochemical mass spectrometry (DEMS) experiments [12,28]. Thus far, no conclusive proof have been found of any synergistic effects regarding activities for chlorine or hydrogen evolution of mixed oxides. Increased activities of mixed coatings have instead been associated with morphological effects [10,11,25]. However, for the more kinetically hindered reaction of oxygen evolution, mixed oxides of $Co_3O_4$ and $RuO_2$ have shown synergistic catalytic effects [9]. In this work, we have studied the kinetic properties of ternary oxide coatings containing the standard 70 mol% $TiO_2$ fraction together with a mixture of ruthenium and cobalt oxides. Since the standard DSA® composition is known to yield coatings of high stability, it is interesting to study mixtures containing both stabilizing $TiO_2$ and active oxides of ruthenium and cobalt. The possible advantages of adding a third oxide could be lower cost and increased stability with a retained activity. To the best of our knowledge, there are no reports on this ternary mixed oxide. Studies concerning the effect of cobalt addition on selectivity and stability of DSA® electrodes are planned for future work.

## 2. Material and methods

We have replaced one third of the ruthenium in the 30:70 Ru:Ti mixture by cobalt, which after calcination resulted in a mixed oxide hereafter referred to as $Ti_{0.7}Ru_{0.3-x}Co_xO_2$, where $x = 0.093$ for the doped samples and 0 for the undoped. Electrodes were made by spin coating onto polished titanium in order to obtain well defined and uniform coating layers [30].

Two coating solutions were prepared using titanium(IV)n-butoxide (TBOT), $RuCl_3 \cdot nH_2O$ (35.51 wt% Ru) and $CoCl_2 \cdot 6H_2O$ as metal precursors. The first solution contained 14.929 g of TBOT and 5.351 g $RuCl_3 \cdot nH_2O$ dissolved in 1-propanol to a final volume of 50 ml, giving a molar ratio between Ti and Ru of 7:3. For the second solution some of the Ru was replaced by an equimolar amount of Co by dissolving 14.929 g TBOT, 3.692 g $RuCl_3 \cdot nH_2O$ and 1.387 g $CoCl_2 \cdot 6H_2O$ in 1-propanol to 50 ml final volume. This gave a molar ratio of Ti:Ru:Co = 7:2.07:0.93. Both solutions were stirred for 48 h to assure complete dissolution of the salts.

These solutions were used to prepare electrodes on polished titanium substrates, and were also investigated by differential scanning calorimetry.

Titanium disks with a diameter of 59 mm, thickness 2.4 mm, were polished to a mirror finish using a Struers Tegra system following a procedure suitable for metallographic preparation of titanium specimens. First, the disks were polished with SiC paper (grit 320) for 2 min, followed by polishing with 9 μm diamond suspension for 5 min, and finished by 40 nm silica suspension for 7 min. After polishing, the substrates were carefully cleaned in an ultrasonic bath and thoroughly rinsed in milli-Q water. The disks were prior to coating pickled in dilute hydrofluoric acid (20 ml concentrated HF per liter $H_2O$) at room temperature for 2 min and again thoroughly rinsed in milli-Q water. To assure that the titanium surfaces were free of water, they were dried at 80 °C for several minutes.

To produce the samples, the prepared substrates were placed in a standard photo-resist spinner (Electronics Micro Systems model 4000). Coating solution was applied to the surface and the substrate was spun with 1400 rpm to distribute an even layer of the solution. The samples were dried at 80 °C for 10 min and calcined at 470 °C. The spin coating procedure was repeated one, three or seven times resulting in 7, 21 or 48 mg oxide on the disk (500, 1450 or 3400 nm thick oxide layers, estimated from weight increase [30]). For the intermediate layers, the calcination of the samples lasted for 10 min, while the final layer was calcined for 1 h. Fig. 1 demonstrates the good reproducibility with the spin-coating technique by showing the weight increase of the samples for each applied coating layer.

The surface structures of the electrodes were studied in scanning electron microscopy (SEM) using a LEO 1450 EP and atomic force microscopy (AFM) using a Digital Instruments Dimension 3100. The morphology of the coatings were examined in transmission electron microscopy (TEM) using a JEOL 2000fx. TEM samples were prepared by scraping the coating off the substrate using a sharp knife and collecting the powder on a grid (Carbon grid 200 mesh). The X-ray diffraction (XRD) measurements were carried out on the doped and undoped sample disk surface at ambient temperature using a Siemens D5000 diffractometer in a grazing incidence set-up with a Göbel mirror and an energy dispersive detector. Cu-$K_\alpha$ ($\lambda = 1.5418$ Å) radiation was used. Scans were performed for the $2\theta$ range 15–75°, with a step size of 0.0092° and 4 s collection time per step. The resulting pattern was imported in the evaluation software package DIFFRAC$^{plus}$EVA with SEARCH, where phases were identified, after background subtraction, with the aid of the ICDD database [31]. Average crystallite size was determined by the Scherrer equation, and measurements in TEM and AFM images.

All electrochemical measurements used Milli-Q water from a Millipore Direct-Q3 water purification system, a Princeton Applied Research PAR 273A potentiostat and a thermostatted cell (25 °C), with a Pt mesh counter electrode. The cell was washed with Milli-Q water between each measurement, and periodically cleaned with a dilute $HNO_3$ solution, and the electrolyte was continuously deaerated with nitrogen gas starting 15 min before each experiment. The reference electrode was connected to the cell via a Luggin capillary. Rotating disk electrodes with an area of 1 $cm^2$ were used, rotating at 3000 rpm during all polarization curve measurements and with no rotation during the cyclic voltammetry. Reference electrodes of two kinds, Ag/AgCl (saturated KCl) (XR300) and Hg/HgO (1 M KOH) (XR400), from Radiometer analytical were used in chloride electrolyte and in NaOH, respectively.

Cyclic voltammetry was performed in 1 M NaOH (Merck, pro analysi). Voltammograms for two electrodes, one containing cobalt and one without cobalt, both with three layers of coating, were measured by sweeping the potential from −1.60 to +1.60 V vs Hg/HgO at a sweep rate of 50 mV/s. Cyclic voltammetry for determination of the surface charge $q^*$ was performed by sweeping the electrode potential from −0.67 to +0.28 V vs Hg/HgO at a sweep rate of 20 mV/s. Numerical integration, using the trapezoidal method, of data for the 10th sweep was used to determine $q^*$.

Polarization curve measurements were performed for anodic or cathodic current densities from 1 to 1000 A/$m^2$, from higher to lower current densities. The current densities were logarithmically spaced, with ten current densities per decade. Anodic current densities were used to yield chlorine evolution from 5 M NaCl (Merck, pro analysi) (adjusted to pH 2 using HCl (Merck, pro analysi)), and cathodic current densities to yield hydrogen evolution from 1 M NaOH. The chloride electrolyte pH was checked using a Metrohm 827 pH lab pH-meter. Before the start of each polarization curve measurement, the working electrode was polarized at −1000 A/$m^2$ for between 3 and 5 min for anodic measurements and for 15 min for cathodic measurements. Then, anodic or cathodic currents were applied, and current interrupt was used to correct for the resistive voltage drops in the system. The overpotential decay transient during 450 μs after each interrupt was recorded using either a Nicolet Pro 10 oscilloscope or a National Instruments (NI) cDAQ 9178 chassis with a NI9223 voltage digitizer. For each applied current density, the mean of 24 transients (when the Nicolet instrument was used) or 72 transients (when the NI instrument was used) were registered. The

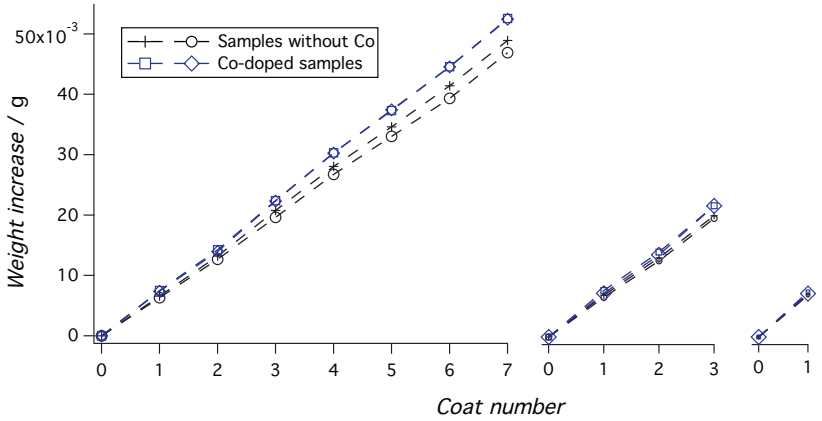


**Fig. 1.** Weight increase as a function of number of coating layers. The weight increase of the samples for each coating layer during the preparation.

following overpotential decay expression, first developed by Morley and Wetmore [32],

$$E = E(t=0) - b \times \ln\left(1 + \frac{t}{\tau}\right) \quad (1)$$

was then fitted to the overpotential decay transient using $(E, t)$ data from each current density. In this expression, $b$ is the Tafel slope of the electrode reaction, $t$ is the time after the current interrupt and $\tau$ is a time constant for the overpotential decay. This fitting yields $E(t=0)$, which is the electrode potential corrected for the ohmic drop in the electrolyte. However, for very low ohmic drops, where the difference between the uncorrected and the corrected potential was less than 5 mV, the uncorrected electrode potential was used. The logarithmic fitting was performed using the open source EzyFit toolbox for MATLAB [33], which interfaces the Nelder–Mead simplex function FMINSEARCH in MATLAB. In this way, the corrected electrode potential for each applied current density was found. These potentials were then used to construct polarization curves. The standard deviation in voltage between two duplicate samples measured in this way was generally less than 10 mV, for both cathodic and anodic measurements. The only exception was for the thinnest coatings, where the standard deviation reached 10–50 mV at current densities lower than 10 A/m$^2$.

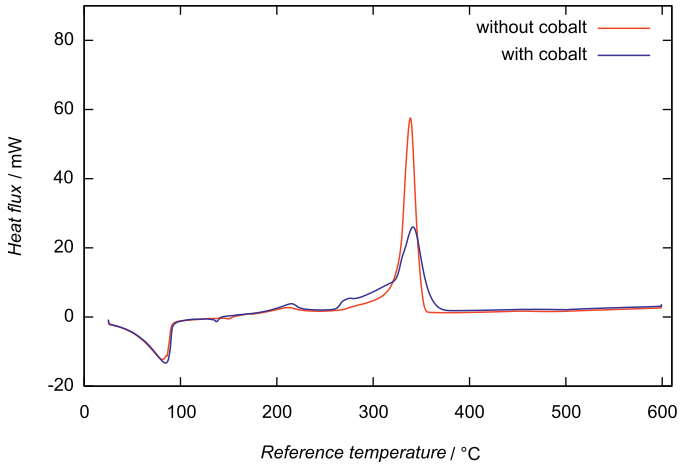


**Fig. 2.** Differential scanning calorimetry. DSC curves of coating solution ($RuCl_3$ + TBOT in 1-propanol) with and without $CoCl_2$ doping, as a function of reference temperature. Measurement performed using a gold crucible, exotherm reaction upwards.

Differential scanning calorimetry (DSC) measurements were performed using a DSC 822e from Metler Toledo. 10 μl of solution was placed in a 40 μl gold crucible, the lid was pierced a few times before sealing. The measurement were performed from 25 °C to

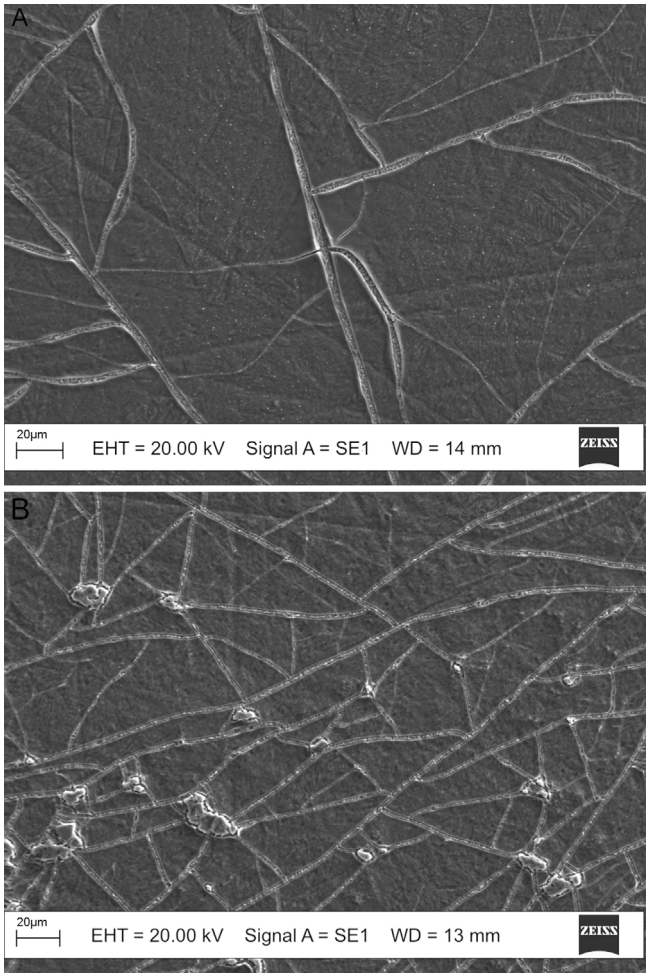


**Fig. 3.** Cracked mud structure. SEM image of cracked mud structure of coating (A) without cobalt and (B) doped with cobalt. There were more cracks per area unit in the cobalt-containing sample. These are one-layer samples (coating thickness approximately 500 nm) and the scratches from the grinding/polishing procedure (visible as faint straight lines) on the substrate was not fully masked by the coating.

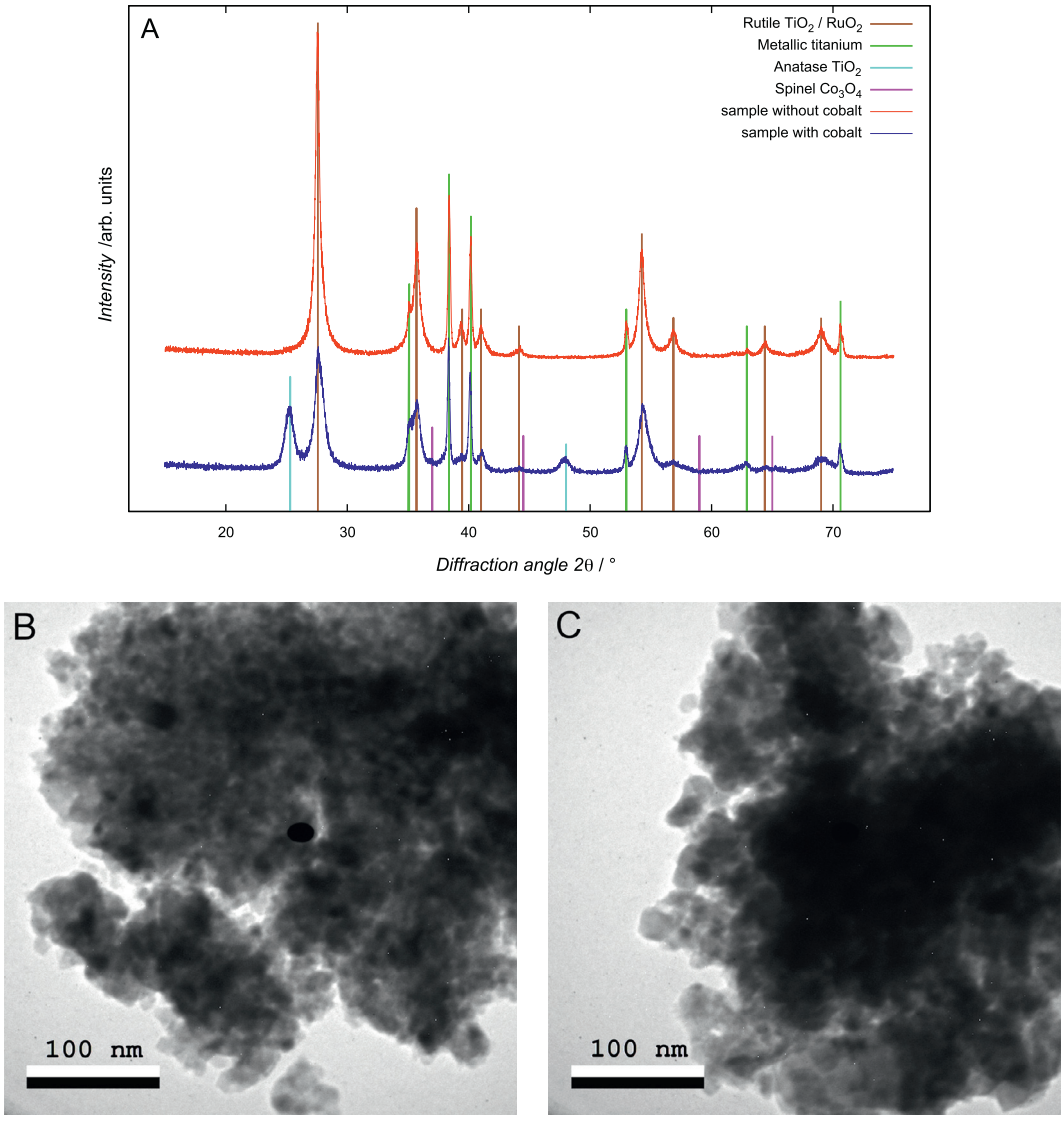


**Fig. 4.** Crystal structure and crystallite size. (A) XRD patterns of $Ti_{0.7}Ru_{0.3-x}Co_xO_2$ ($x = 0$ and 0.093) spin coated onto titanium disks. The curves are vertically offset for clarity. Coating thickness was approximately 3400 nm (7 layers). The magenta vertical lines marks the angles where the $Co_3O_4$ spinel peaks should have appeared. (B) and (C) TEM images of coating oxide with and without cobalt doping (grain size approximately 10 and 20 nm, in agreement with estimates from XRD data), respectively. The black elliptic dot in the center is an imaging artifact.

600 °C at a heating rate of 5 °C/min. As reaction gas 50 ml/min of air was used (inlet temperature: 21 °C; relative humidity: 23.8%).

## 3. Results and discussion

### 3.1. Differential scanning calorimetry

Fig. 2 shows the DSC curves from the two coating solutions used in the study. The results have been verified using both gold and aluminum crucibles, so it is unlikely that any part of the curve can be explained as reactions between the solution and the crucible material. The endothermic feature below 100 °C is present in both curves, and could be straightforwardly attributed to the evaporation of solvent. The main features of the curves was found in the temperature interval 270–380 °C. These were attributed to oxidation of the precursors and formation of the oxide coating material. When comparing the two curves, it can be seen that the oxidation of the solution doped with cobalt peaked at a slightly higher temperature than the oxidation of the undoped coating solution ($T_c$ increased from 338 °C to 341 °C). Also to be noted is that the oxidation took place over a larger temperature interval and showed lower heat release in the presence of cobalt. No reactions were detected in the temperature range of 380–600 °C. For comparison, we have also performed DSC experiments on a solution of only cobalt chloride in 1-propanol (1.387 g $CoCl_2 \cdot 6H_2O$ dissolved in 1-propanol to 50 ml final volume) using the same procedure (data not shown). This curve displayed the same initial solvent evaporation, but was then completely flat for all temperatures up to 600 °C. In other words, $CoCl_2$ in propanol did not oxidize in the range of less than 600 °C, which is in contrast to Louardi et al. [34] who have obtained $Co_3O_4$ from $CoCl_2$ in water by spray pyrolysis at 350 °C, and Garavaglia et al. [19] who have obtained $Co_3O_4$ by thermal decomposition of $CoCl_2 \cdot 6H_2O$ at 400 °C when the duration time was long enough (>10 h). The lower heat release of the oxidation of the cobalt containing solution was not surprising. The standard enthalpies of formation for the oxides and chlorides of the involved metals can be found in standard reference tables [35] to be −205 kJ/mol for $RuCl_3$, −205 kJ/mol for $RuO_2$, −312 kJ/mol for $CoCl_2$, −238 kJ/mol for CoO and −891 kJ/mol for $Co_3O_4$. In other words, the oxidation reaction $3CoCl_2 + 2O_2 \rightarrow Co_3O_4 + 3Cl_2$ is endothermic

($\Delta H$ = +46 kJ/mol), as is the reaction $CoCl_2 + 0.5O_2 \rightarrow CoO + Cl_2$ ($\Delta H$ = +74 kJ/mol). On the contrary, the corresponding reaction for ruthenium, $RuCl_3 + O_2 \rightarrow RuO_2 + 1.5Cl_2$ is exothermic ($\Delta H$ = −100 kJ/mol). Therefore, it is expected that the formation of a mixture of Ti, Ru and Co oxides should release less heat than the formation of a mixture of only Ti and Ru oxides.

### 3.2. Surface morphology

Doping with cobalt affected the cracked-mud structure of the $(Ti,Ru)O_2$ mixed oxide so that the crack-density increased (Fig. 3). The effect was most distinct for the thinnest (0.5 μm) coating and were hardly present for the thickest (3 μm) coating. Also, in the intersections of the cracks of the doped coating, there were some very small plaquettes that were not seen on the undoped samples. Da Silva et al. [11] characterized the surface properties of the $(RuO_2)_x + (Co_3O_4)_{(1-x)}$ system and found that if the amount of $Co_3O_4$ is less than 50 mol%, the electrode is indistinguishable from the pure $RuO_2$ electrode using SEM. However, they did find an increase in the crack-density for higher cobalt concentrations.

### 3.3. Crystallinity

The $(Ru,Ti)O_2$ mixed oxide doped with cobalt showed smaller grains compared to the undoped oxide. Average crystallite size, estimated from XRD (the pattern is displayed in Fig. 4) using the Scherrer equation for the main peaks at $2\theta = 27.67^\circ$ and $27.53^\circ$ respectively, was 10 nm for the sample with cobalt and 20 nm for the sample without. The size estimation was confirmed by measurements in TEM (Fig. 4) and AFM images (Fig. A.1 in supplementary information). This gave a real area for the doped sample that was about twice the area of the undoped (Eq. (2)).

$$A_{tot} = \frac{1}{V} \cdot A \propto \frac{1}{r^3} \cdot r^2 = \frac{1}{r} \quad (2)$$

The area enlargement was calculated under the assumption of monocrystalline symmetrical grains of homogeneous size [36] in each sample. The smaller grains of the doped sample was in contradiction with Jirkovský et al. [28] who found that $RuO_2$ doped with cobalt in fact have larger grains than the undoped $RuO_2$. Their study is however of a binary oxide without titanium and with nitrate precursors which could explain the difference. Garavaglia et al. [19] studied the physical properties of $Co_3O_4$ prepared from $CoCl_2$ and $Co(NO_3)_2$ and concluded that $CoCl_2$ is not a good starting point if one is to obtain small crystals, in analogy with the $RuO_2$ case [36]. The effect of the precursor on the ternary mixed oxide have not been investigated further. In the cobalt doped $TiO_2$ binary oxide case, Li et al. [37] found that the doping does not affect the particle size (calculated from Brunauer–Emmett–Teller (BET) surface area).

The undoped $(Ti,Ru)O_2$ oxide displayed mainly rutile structure in agreement with Comninellis and Vercesi [38]. $Co_3O_4$ (spinel structure) is the thermodynamically preferred cobalt oxide in films prepared from solutions [39], but no spinel peak was observed in the XRD data. The only difference between the two samples is the existence of $TiO_2$ in anatase (PDF 01-086-1157 [31]) in the cobalt doped sample. This led to the conclusion that the cobalt must have entered the overall rutile structure of the $(Ti,Ru)O_2$ as suggested by Li et al. [37]. It might also exist as an amorphous compound. This did not agree with most reports on mixed oxides of ruthenium and cobalt [8–11] as they refer to the spinel structure together with the rutile, but agreed with Makarova et al. [12] who only found the spinel structure in their sample when the annealing temperature had been very high (900 °C). Da Silva et al. [11] explains the lack of spinel peaks in the diffractogram for high ruthenium concentration

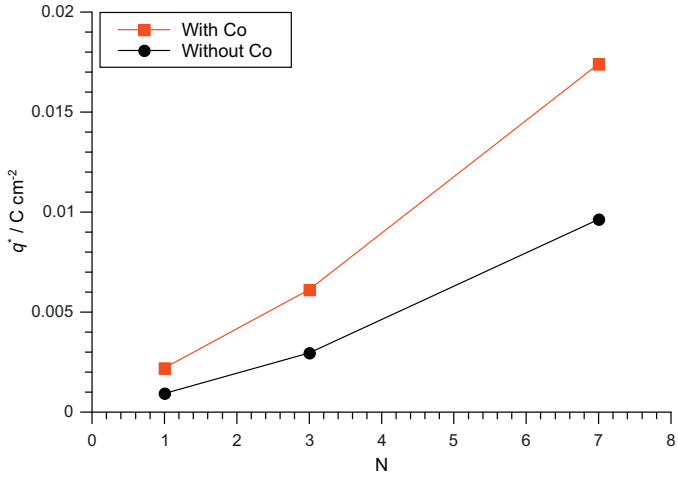


**Fig. 5.** Voltammetric charge. The voltammetric charge, $q^*$, versus the number of applied coating layers.

mixtures (>70 mol%) by the highly amorphous nature of their film, and interpreted the amorphous state as an indication of insolubility of $Co_3O_4$ in $RuO_2$. Since our oxide film was not highly amorphous that explanation of the non-existing spinel peaks is unlikely, and we have shown that it is possible to solve cobalt in ruthenium–titanium dioxide in another crystalline form than $Co_3O_4$. Jirkovský et al. [28] found spinel in samples annealed at 400 °C only when the Co:Ru ratio was larger than 2:1. Their less cobalt-containing samples were all of a single phase (rutile).

### 3.4. Cyclic voltammetry

The calculated voltammetric charge, $q^*$, versus the number of layers applied is shown in Fig. 5. Data from the 10th sweep, where the voltammograms indicated that the electrodes had reached steady state, was used in all cases. The voltammetric charge for the doped coatings is about twice as high as that of the undoped samples, which is in agreement with results on coatings of $RuO_2$ and of $RuO_2 + Co_3O_4$ having the same molar ratio as in the present study (Ru:Co of 2:1) [10] and indicates a higher active surface area for the doped electrodes.

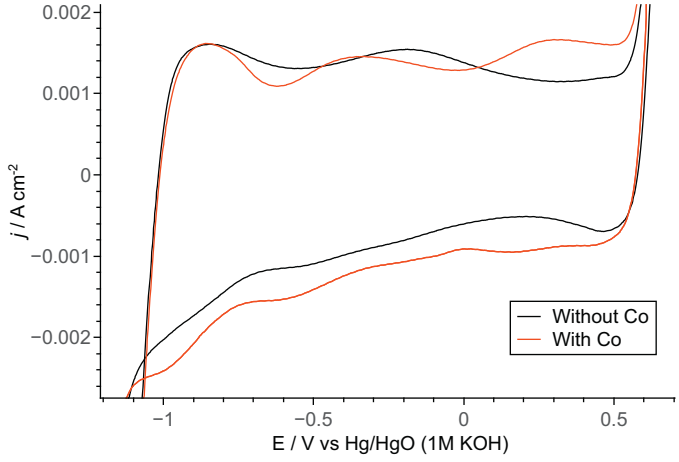


**Fig. 6.** Broad cyclic voltammograms. Broad cyclic voltammogram in 1 M NaOH. There are significant differences between coatings with and without cobalt. Specifically, the doped coating exhibited an anodic peak at 0.3 V vs Hg/HgO. Hydrogen evolution occurs at potentials below −1 V vs Hg/HgO and oxygen evolution at potentials above 0.6 V vs Hg/HgO. The potential was swept between −1.6 V and 1.6 V vs Hg/HgO at 50 mV/s.

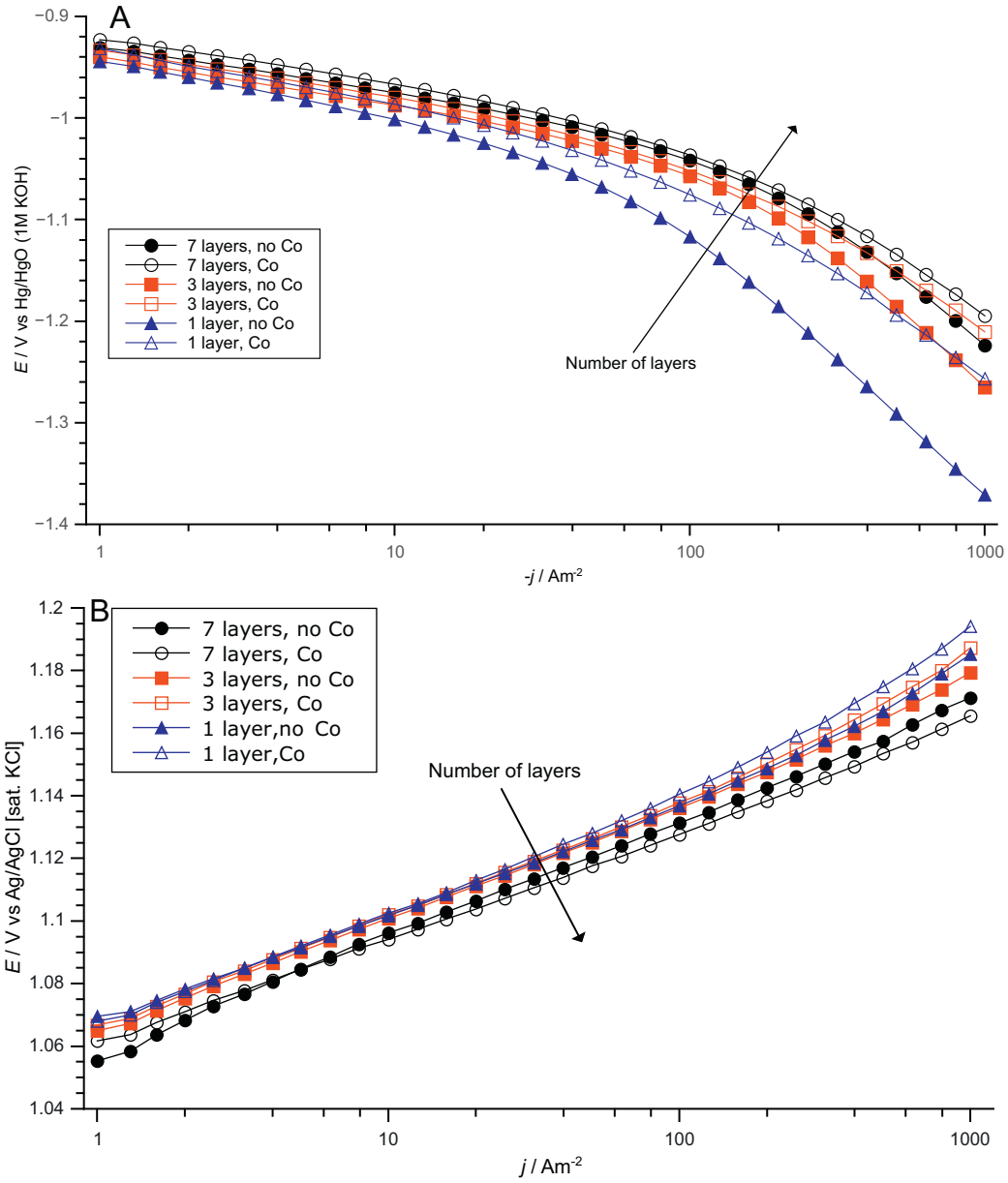


**Fig. 7.** Polarization curves. (A) Cathodic polarization curves for hydrogen evolution from 1 M NaOH. (B) Anodic polarization curves for chlorine evolution from 5 M NaCl solution.

The magnitude of the voltammetric charge is hard to compare with previous work, since different parts of the voltammograms have been used to calculate $q^*$. Trasatti [26] and Krstajić and Trasatti [25] found voltammetric charges for binary ruthenium–cobalt oxide coatings of the same order of magnitude as those of the thickest electrode coatings examined here. However, the binary coatings examined by Da Silva et al. [11] exhibited voltammetric charges about ten times as large as those of the present coatings. All previous studies of binary ruthenium–cobalt oxides have used electrodes prepared using brush- or dip coating, but not spin coating as in the present work.

Cyclic voltammograms recorded between the onset potentials for hydrogen evolution and oxygen evolution are shown in Fig. 6. The voltammogram for the undoped sample is similar to that reported for $RuO_2$ [40], whereas the CV for the cobalt doped coating show an additional anodic peak at around 0.3 V vs Hg/HgO. This peak is partially included in the voltage range used for the calculation of $q^*$ (see Fig. 5), influencing the calculated value of the voltammetric charge.

Previous studies [23,25] performed in alkaline solutions have, based on Pourbaix diagrams for cobalt [42], identified a peak at a potential corresponding to 0.5 V vs Hg/HgO. Boggio et al. [23] related this peak to the oxidation of surface cobalt compounds to Co(IV) according to

$$CoOOH \rightarrow CoO_2 + H^+ + e^- \quad (3)$$

It has been found, for binary ruthenium–cobalt oxide coatings, that increasing the content of ruthenium decreases the peak related to reaction (3) without changing the potential at which it occurs [25]. In the present case, the voltammograms show a peak unique to the ternary cobalt doped coating at 0.3 V vs Hg/HgO, likely related to Co oxidation.

### 3.5. Polarization curves

Polarization curves for hydrogen and chlorine evolution are seen in Fig. 7 where each marker represents the mean of two measurements on duplicate electrodes.

The polarization curves for hydrogen evolution (Fig. 7A) exhibit two distinct regions, as has also been seen in previous studies of $RuO_2$ [40]. The Tafel slopes in region I (at lower applied current densities) are −55 to −60 mV/dec, irrespective of doping, which is in the range of 40–60 mV/dec typical for hydrogen evolution on ruthenium dioxide in alkaline electrolyte [24,40,41]. Note that the corresponding slope on coatings of 100% $Co_3O_4$ was found to be higher, 105 mV/dec [24].

In region II (at current densities from about 100 $A/m^2$), the cobalt doped electrodes show lower Tafel slopes than the undoped electrodes, in particular for thinner coatings. The slope for undoped electrodes in region II changes from 0.22 V/dec for electrodes with 7 layers of coating, to 0.26 V/dec for 3 layer coatings and 0.27 V/dec for the thinnest coating. For doped coatings, the Tafel slope for both 7 and 3 layer electrodes was almost the same, at around 0.19 V/dec, increasing to 0.21 V/dec for 1 layer coatings. This difference in Tafel slope between doped and undoped electrodes yields a significantly lower overvoltage for the doped coatings at current densities approaching industrial levels.

For chlorine evolution, the Tafel slopes and overpotentials are similar for all electrodes. There is a general tendency of lower overpotentials for thicker electrode coatings, in agreement with previous work [2,39,40]. The Tafel slopes between 10 and 1000 $A/m^2$ are, regardless of doping and coating thicknesses, 35 to 45 mV/dec, which is typical for both $Co_3O_4$ [22] and $RuO_2$ [1] in acidic solution. To examine if a synergistic effect of the doping is present, polarization curves normalized with respect to surface area as measured by the voltammetric charge have been prepared for both hydrogen evolution and chlorine evolution (curves are presented in the supplementary information). These curves indicate that the active surface area of the electrodes have a key influence on the overpotentials, and that for electrodes with the same coating thickness, doped electrodes exhibit lower normalized current densities at a certain electrode potential. Thus the activity, when corrected for the active surface area, is lower for doped electrodes. Synergistic effects between Co, Ru and Ti in ternary mixed coatings do not seem to be present and the lower overpotentials for hydrogen evolution in region II exhibited by doped electrodes could thus be explained by the increased electrochemical surface area of these samples. The same factor can explain why doped coatings showed essentially the same Tafel slope and overpotential in region I of the hydrogen evolution polarization curve, and in the chlorine evolution polarization curves, as undoped samples. These results give further support to the interesting possibility of reducing the amount of Ru in DSA® coatings by doping with cobalt.

Except for adhesion tests using normal office Scotch tape, we did not perform any regular stability measurements. The tape tests did however show excellent adhesion for all samples. Moreover, in SEM and AFM images the electrodes appeared to have similar morphology regardless of the doping. The increased porosity is not visible in any other way than the smaller grains of the doped samples (that is, no larger pores were observed). The packing of the grains was similar in all electrodes and in none of the samples the grains were detached or displaced by the AFM tip.

## 4. Conclusions

Cobalt doped DSA® electrodes exhibited higher activity for hydrogen evolution than undoped electrodes at current densities approaching industrial levels, even though containing only two thirds as much active ruthenium. The activity for chlorine evolution was similar for the two coating types. Doping with cobalt approximately doubled the surface area of the electrodes, as estimated from measurements of grain sizes and voltammetric charges, and this increased area explained the high activity of the cobalt containing coatings. The crack density on the micrometer scale also increased by the cobalt doping, at least for thin coatings, but the excellent coating adhesion was not affected. The cobalt does not form $Co_3O_4$ phase, but is rather incorporated in the overall rutile structure of the $(Ru,Ti)O_2$.

## Authors' contribution

Authors CH and RKBK have contributed equally. Conceived and designed the study: CH, JB. Sample preparation: RKBK, JB. Designed and performed the experiments: CH, RKBK, SMHR. Analyzed the data: CH, RKBK, JB, SMHR, AC, SE, HO. Wrote the paper: CH, RKBK, AC, JB, HO.

## Role of the funding sources

This work is part-financed by the European Regional Development Fund through the project "Energywise", the Swedish Research Council, the Swedish Energy Agency, Permascand AB and Länstyrelsen Västernorrland. The funders had no role in study design, data collection and analysis, decision to publish, or preparation of the manuscript.

## Acknowledgements

Susanne Holmin is acknowledged for fruitful discussions.

## Appendix A. Supplementary data

Supplementary data associated with this article can be found, in the online version, at http://dx.doi.org/10.1016/j.mseb.2013.08.018.

## References

[1] S. Trasatti (Ed.), Electrodes of Conductive Metallic Oxides: Part A, Elsevier, Amsterdam, 1980.
[2] S. Trasatti, Electrochim. Acta 45 (2000) 2377–2385.
[3] L.A. DeFaria, J.F.C. Boodts, S. Trasatti, Electrochim. Acta 37 (1992) 2511–2518.
[4] N. Buné, V.V. Losev, M.F. Reznik, E. Zaripova, Soviet Electrochem. 22 (1986) 365–368.
[5] H.B. Beer, British Patent 1,195,871 (1967).
[6] S. Hosokawa, H. Kanai, K. Utani, Y. Taniguchi, Y. Saito, S. Imamura, Appl. Catal. B - Environ. 45 (2003) 181–187.
[7] M. Ito, Y. Murakami, H. Kaji, K. Yahikozawa, Y. Takasu, J. Electrochem. Soc. 143 (1996) 32–36.
[8] Y. Liu, W. Zhao, X. Zhang, Electrochim. Acta 53 (2008) 3296–3304.
[9] L.M. Da Silva, J.F.C. Boodts, L.A. De Faria, Electrochim. Acta 46 (2001) 1369–1375.
[10] L.M. Da Silva, J.F.C. Boodts, L.A. De Faria, J. Braz. Chem. Soc. 14 (2003) 388–395.
[11] L.M. Da Silva, J.F.C. Boodts, L.A. De Faria, Electrochim. Acta 45 (2000) 2719–2727.
[12] M.V. Makarova, J. Jirkovský, M. Klementová, I. Jirka, K. Macounová, P. Krtil, Electrochim. Acta 53 (2008) 2656–2664.
[13] K. Macounová, J. Jirkovský, M.V. Makarova, J. Franc, P. Krtil, J. Solid State Electrochem. 13 (2009) 959–965.
[14] Y. Takasu, S. Onoue, K. Kameyama, Y. Murakami, K. Yahikozawa, Electrochim. Acta 39 (1994) 1993–1997.
[15] D.T. Shieh, B.J. Hwang, Electrochim. Acta 38 (1993) 2239–2246.
[16] T.A.F. Lassali, J.F.C. Boodts, S. Trasatti, Electrochim. Acta 39 (1994) 1545–1549.
[17] J.L. Fernandez, M.R.G. De Chialvo, A.C. Chialvo, J. Appl. Electrochem. 32 (2002) 513–520.
[18] R.A. Agapova, G.N. Kokhanov, Elektrokhimiya 12 (1976) 1649–1653.
[19] R. Garavaglia, C.M. Mari, S. Trasatti, Surf. Technol. 19 (1983) 197–215.
[20] R. Garavaglia, C.M. Mari, S. Trasatti, Surf. Technol. 23 (1984) 41–47.
[21] S. Trasatti, Electrochim. Acta 29 (1984) 1503–1512.
[22] R. Boggio, A. Carugati, G. Lodi, S. Trasatti, J. Appl. Electrochem. 15 (1985) 335–349.
[23] R. Boggio, A. Carugati, S. Trasatti, J. Appl. Electrochem. 17 (1987) 828–840.
[24] N. Krstajić, S. Trasatti, J. Appl. Electrochem. 28 (1998) 1291–1297.

[25] N. Krstajić, S. Trasatti, J. Electrochem. Soc. 142 (1995) 2675–2681.
[26] S. Trasatti, in: R.W. Curry (Ed.), Modern Chlor-Alkali Technology, vol. 6, Royal Society of Chemistry, Cambridge, 1995.
[27] L.M. Da Silva, L.A. De Faria, J.F.C. Boodts, J. Electroanal. Chem. 532 (2002) 141–150.
[28] J. Jirkovský, M. Makarova, P. Krtil, Electrochem. Commun. 8 (2006) 1417–1422.
[30] C. Hummelgård, J. Gustavsson, A. Cornell, H. Olin, J. Bäckström, Thin Solid Films 536 (2013) 74–80.
[31] S. Kabekkodu (Ed.), ICDD. PDF-4+2010 (Database), International Centre for Diffraction Data, Newtown Square, 2010.
[32] H. Morley, F. Wetmore, Can. J. Chem. 34 (1956) 359–363.
[33] F. Moisy, EzyFit, a free curve fitting toolbox for MATLAB, Version 2.4. http://www.fast.u-psud.fr/ezyfit/
[34] A. Louardi, A. Rmili, F. Ouachtari, A. Bouaoud, B. Elidrissi, H. Erguig, J. Alloys Compd. 509 (2011) 9183–9189.
[35] D.R. Lide (Ed.), CRC Handbook of Chemistry and Physics, 89th edition, CRC Press, Boca Raton, 2008.
[36] C. Malmgren, A.K. Eriksson, A. Cornell, J. Bäckström, S. Eriksson, H. Olin, Thin Solid Films 518 (2010) 3615–3618.
[37] J.G. Li, R. Büchel, M. Isobe, T. Mori, T. Ishigaki, J. Phys. Chem. C 113 (2009) 8009–8015.
[38] C. Comninellis, G.P. Vercesi, J. Appl. Electrochem. 21 (1991) 335–345.
[39] S. Ardizzone, G. Fregonara, S. Trasatti, Electrochim. Acta 35 (1990) 263–267.
[40] A. Cornell, D. Simonsson, J. Electrochem. Soc. 140 (1993) 3123–3129.
[41] D. Miousse, A. Lasia, J. New Mater. Electrochem. Syst. 2 (1999) 71–78.
[42] E. Deltombe, M. Pourbaix, Cobalt, Pergamon Press Ltd., 1966, pp. 322–329.